Physics of transport in tokamaks

INSTITUTE OF PHYSICS PUBLISHING PLASMA PHYSICS AND CONTROLLED FUSION

Plasma Phys. Control. Fusion **46** (2004) B557–B574 PII: S0741-3335(04)85422-8

Physics of transport in tokamaks

X Garbet[1], P Mantica[2], C Angioni[3], E Asp[1], Y Baranov[4], C Bourdelle[1], R Budny[5], F Crisanti[6], G Cordey[4], L Garzotti[7], N Kirneva[8], D Hogeweij[9], T Hoang[1], F Imbeaux[1], E Joffrin[1], X Litaudon[1], A Manini[3], D C McDonald[4], H Nordman[10], V Parail[4], A Peeters[3], F Ryter[3], C Sozzi[2], M Valovic[4], T Tala[11], A Thyagaraja[4], I Voitsekhovitch[4], J Weiland[10], H Weisen[12], A Zabolotsky[12] and the JET EFDA Contributors

[1] Assoc. EURATOM-CEA, CEA/DSM/DRFC CEA-Cadarache, 13108 Saint Paul Lez Durance, France
[2] Istituto di Fisica del Plasma EURATOM-ENEA/CNR, via Cozzi 53, 20125 Milano, Italy
[3] MPI für Plasmaphysik, EURATOM-Assoz., D-8046 Garching bei München, Germany
[4] EURATOM/UKAEA, Culham Science Centre, Abingdon OX14 3DB, UK
[5] PPPL, Princeton University, PO Box 451, Princeton, NJ 08543, USA
[6] Assoc. EURATOM-ENEA sulla Fusione, Via Enrico Fermi 27, 00044 Frascati, Italy
[7] EURATOM-ENEA-CNR Association, Istituto Gas Ionizzati, Padova, Italy
[8] RRC Kurchatov Institute, Moscow, Russia
[9] FOM-Instituut voor Plasmafysica, Associatie EURATOM-FOM, Nieuwegein, The Netherlands
[10] Chalmers University of Technology and EURATOM-VR Assoc, S-41296 Göteborg, Sweden
[11] Association EURATOM-TEKES, VTT Processes, FIN-02044 VTT, Finland
[12] Assoc. EURATOM-Confédération Suisse, CRPP, EPFL, CH-1015 Lausanne, Switzerland

Received 2 July 2004
Published 17 November 2004
Online at stacks.iop.org/PPCF/46/B557
doi:10.1088/0741-3335/46/12B/045

Abstract

This paper is an overview of recent results relating to turbulent particle and heat transport, and to the triggering of internal transport barriers (ITBs). The dependence of the turbulent particle pinch velocity on plasma parameters has been clarified and compared with experiment. Magnetic shear and collisionality are found to play a central role. Analysis of heat transport has made progress along two directions: dimensionless scaling laws, which are found to agree with the prediction for electrostatic turbulence, and analysis of modulation experiments, which provide a stringent test of transport models. Finally the formation of ITBs has been addressed by analysing electron transport barriers. It is confirmed that negative magnetic shear, combined with the Shafranov shift, is a robust stabilizing mechanism. However, some well established features of internal barriers are not explained by theory.

(Some figures in this article are in colour only in the electronic version)

1. Introduction

Understanding transport in magnetized plasmas is a subject of utmost importance for the design of future fusion reactors. A vigorous and coordinated effort has been undertaken in Europe to

improve our knowledge in this domain. This paper is an overview of recent results that clarify the questions of turbulent particle and heat transport, and conditions for the onset of internal transport barriers (ITBs). The aim is to compare theoretical and experimental results for each of these topics and to assess the implications for burning plasmas.

Particle transport is a central question, since fusion power increases as the square of the density. Therefore the existence and nature of any process that leads to density peaking deserves attention. Recently the theory of turbulent pinches has made significant progress. In particular the role of collisionality and magnetic shear has been clarified. These predictions have been tested against experiments on JET, ASDEX-Upgrade, TORE SUPRA and TCV.

The understanding of heat transport has advanced in two directions: dimensionless scaling laws and assessment of transport models using heat modulation experiments. Scaling laws are widely used to predict the energy confinement time in next step devices. When written in dimensionless form, they also yield information on the mechanisms that underlie turbulent transport. Profile modelling plays an increasing role in interpreting existing data and in the design of future experiments. Therefore the predictive capability of transport models is a central issue. A powerful means of testing these models is to use heat modulation experiments. Such experiments have been undertaken, analysed and compared on JET, ASDEX-Upgrade, TORE SUPRA, FTU and TCV.

Finally, triggering ITBs with a low power threshold is also a challenge for future devices. This is a delicate question since turbulent transport results from a balance between driving terms (gradients) and a combination of stabilizing effects such as magnetic and velocity shears. Electron transport barriers are well suited to studying this physics. In this case the electron temperature gradient becomes large, whereas the density, velocity and ion temperature gradients (ITGs) remain small and so, therefore, does the perpendicular velocity shear rate. The magnetic shear is a key parameter in many cases, as found in JET, ASDEX-Upgrade, TORE SUPRA, FTU and TCV. Theory broadly supports this picture. However, some robust features of internal barriers are not understood, in particular the role of certain values of the safety factor and the existence of multiple barriers observed in JET. Some possible explanations will be presented in this paper.

The remainder of this paper is organized as follows. Section 2 briefly presents some general features and properties of drift wave turbulence in core tokamak plasmas. Particle transport is addressed in section 3, profile stiffness in section 4 and ITBs in section 5. A conclusion follows.

2. A brief survey of micro-stability and turbulent transport

This paper is based on a restricted theory of turbulent transport where turbulence is driven by two main electrostatic micro-instabilities: ITG-driven modes and trapped electron modes (TEMs) [1, 2] (called here ion and electron modes for simplicity). This assumption is appropriate if the plasma $\beta = 2\mu_0 p/B^2$ (p is the total pressure and B the magnetic field) is low enough to ignore electromagnetic effects, in particular if it is lower than the instability threshold of kinetic ballooning modes [3]. Also the electron temperature profile is assumed to be stable with respect to small scale electron temperature gradient driven modes [4]. ITG/TEM modes are unstable in the limit of large wavelengths such that $k_\perp \rho_\mathrm{i} < 1$, where $k_\perp$ is the perpendicular wave number and ρ_i is the ion Larmor radius ($\rho_\mathrm{i} = (m_\mathrm{i} T_\mathrm{i})^{1/2}/eB$, where m_i is the ion mass and T_i is the ion temperature). In the non-linear regime, they produce particle, momentum, electron and ion heat transport. An important feature of these micro-modes is the existence of an instability threshold. In a deuterium plasma, and for a given profile of the safety factor, the threshold of a pure ion mode (i.e. adiabatic electrons) appears as a critical

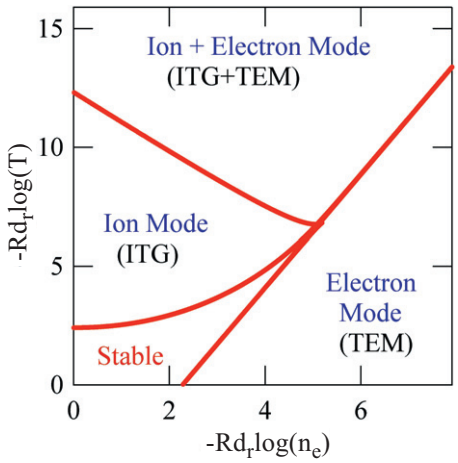

Figure 1. Stability diagram of ITG/TEM modes. Electron and ion temperatures are equal.

ion temperature logarithmic gradient $-R\nabla T_\mathrm{i}/T_\mathrm{i}$ (R is the major radius) that depends on the logarithmic density gradient $-R\nabla n_\mathrm{e}/n_\mathrm{e}$ and on the ratio of electron to ion temperature $T_\mathrm{e}/T_\mathrm{i}$. An ion mode usually rotates in the ion diamagnetic direction (the ion diamagnetic velocity is $\boldsymbol{V}^*_\mathrm{pi} = \boldsymbol{B}\times\boldsymbol{\nabla}p_\mathrm{i}/n_\mathrm{i}e_\mathrm{i}B^2$, where p_i is the ion pressure, n_i the ion density). TEMs usually rotate in the electron diamagnetic direction and are mainly driven through a resonant interaction of the modes with trapped electrons at the precession frequency. The threshold is a critical value of $-R\nabla T_\mathrm{e}/T_\mathrm{e}$ that depends on $-R\nabla n_\mathrm{e}/n_\mathrm{e}$ and the fraction of trapped electrons f_t. A separate treatment of ion and electron modes is usually an oversimplification. Nevertheless, there exist experimental situations where one branch is dominant, for instance when one species is hotter than the other. Figure 1 shows an example of a stability diagram in the special case where the electron and ion temperatures are equal, $T_\mathrm{e} = T_\mathrm{i}$. Depending on the values of gradient lengths, 0, 1 or 2 modes may be unstable. The sign of the phase velocity is not an unambiguous signature of the type of mode that is excited. Typically, the region of large density gradients in the stability domain is dominated by electron modes, whereas for a flat density profile, the first unstable mode is an ion mode. These micro-instabilities are, in essence, interchange modes. Well above all thresholds, both branches combine and the growth rate is of the form

$$\gamma_0^2 = f_\mathrm{t}\omega_\mathrm{de}\omega^*_\mathrm{pe} + \omega_\mathrm{di}\omega^*_\mathrm{pi}, \tag{1}$$

where $\omega^*_\mathrm{ps} = k_\theta V^*_\mathrm{ps}$ and $\omega_\mathrm{ds} = 2k_\theta\lambda_\mathrm{s}V_\mathrm{ds}$ (V_ds is the vertical drift velocity, $V_\mathrm{ds} = -2T_\mathrm{s}/e_\mathrm{s}BR$, $k_{\theta'}$ is a poloidal wave number, and $\boldsymbol{V}^*_\mathrm{ps} = \boldsymbol{B}\times\boldsymbol{\nabla}p_\mathrm{s}/n_\mathrm{s}e_\mathrm{s}B^2$ is the diamagnetic velocity of the species 's'). For trapped electrons, $\lambda_\mathrm{e} = 1/4 + 2s/3$ characterizes the dependence of the precession frequency on magnetic shear s, where $s = \mathrm{d}\log(q)/\mathrm{d}\log(r)$. For ions, $\lambda_\mathrm{i} = \langle\cos(\theta) + s\theta\sin(\theta)\rangle$, where the bracket indicates an average over the mode poloidal structure.

First principle transport models such as Weiland *et al* [5] or GLF23 [6] models are essentially based on linear stability. They provide quantitative fluxes following two separate steps. The first one is based on a quasi-linear expression of fluxes. Considering for instance the particle flux $\Gamma_\mathrm{e} = \langle n_\mathrm{e}v_\mathrm{Er}\rangle$, where $\boldsymbol{v}_\mathrm{E}$ is the $E\times B$ drift velocity ('electrostatic' turbulence), it reads in Fourier space as

$$\Gamma_\mathrm{e} = \sum_{k\omega} n_{\mathrm{e},k\omega}\frac{\mathrm{i}k_\theta\phi^*_{k\omega}}{B}, \tag{2}$$

where $\phi_{\boldsymbol{k}\omega}$ and $n_{\boldsymbol{k}\omega}$ are Fourier components of perturbed electric potential and density. The quasi-linear expression consists in replacing the Fourier component of the density by its linear expression calculated with linearized fluid or kinetic equations. Assuming a convection equation $\partial_t n_e + \boldsymbol{\nabla} \cdot (n_e \boldsymbol{v}_E) = 0$ and a uniform magnetic field (implying incompressibility $\boldsymbol{\nabla} \cdot \boldsymbol{v}_E = 0$), the recipe given above yields a diffusive law $\Gamma_e = -D_{ql}\, \mathrm{d}n_e/\mathrm{d}r$. The quasi-linear diffusion coefficient D_{ql} is given by the expression

$$D_{ql} = \sum_{\boldsymbol{k}\omega} \left| \frac{k_\theta \phi_{\boldsymbol{k}\omega}}{B} \right|^2 \tau_{c,\boldsymbol{k}}, \tag{3}$$

where $\tau_{c,\boldsymbol{k}}$ is a correlation time. This expression can be understood as a random walk estimate. A similar exercise can be carried out for electron (respectively ion) heat flux $\phi_{Ee} = 3/2\langle p_e v_{Er}\rangle$ (respectively $\phi_{Ei} = 3/2\langle p_i v_{Er}\rangle$), leading to a thermal diffusivity $\chi_{e,i} = 3/2 D_{ql}$. In fact an advection equation is too simple, and the whole set of fluid or kinetic linearized equations must be kept when calculating the quasi-linear fluxes, as done in the Weiland and GLF23 models. Equation (3) depends on the level of potential fluctuations, which is unknown at this stage.

The second step consists in using a mixing-length rule to determine the level of fluctuations. The simplest version of this rule is $e\phi_{k\omega}/T_e = 1/k_\perp L_p$ (L_p is a pressure gradient length), which can be modified in various ways to account for the complex nonlinear features of turbulence [2]. This approximation is certainly the weakest part of the derivation of any transport model.

An important feature of turbulent transport is the existence of a similarity principle, which states that three dimensionless parameters, among many others, play a central role [7, 8]. These are the normalized gyroradius $\rho_* = \rho_i/a$ (a is the minor radius), collisionality $\nu^* = \nu_{ei} q R/\varepsilon_a^{3/2} v_{Te}$ (ν_{ei} the electron–ion collision frequency, $\varepsilon_a = a/R$ is the inverse aspect ratio, v_{Te} is the thermal electron velocity), and plasma beta β. Turbulence simulations indicate that the scaling law is 'gyroBohm' for small enough values of ρ_*. This means that correlation lengths, correlation times and diffusivity scale, respectively, as ρ_i, R/v_{Ti} and $\rho_* T_i/eB$ (v_{Ti} is the ion thermal speed $(T_i/m_i)^{1/2}$). The situation is less clear for β and collisionality parameters, because of competing effects. Collisionality has a stabilizing effect on electron (TEM) modes due to electron collisional detrapping [9]. On the other hand, collisional friction damps zonal flows [10, 11], which are fluctuations of poloidal velocity that reduce turbulent transport. The parameter β controls both the compression of magnetic surfaces (the Shafranov shift, which is stabilizing, see section 5.2) and the excitation of electromagnetic instabilities [3]. Hence no β dependence is expected if turbulence is electrostatic and Shafranov shift stabilization is negligible (typically well below the ideal MHD stability limit).

This overview will address plasmas in the L- or H-mode. The L-mode is the reference case where transport is turbulent everywhere. The H-mode is a regime of improved confinement, which results from a quenching of turbulence localized at the plasma periphery. This improvement leads to the formation of a pedestal in density and temperature. Electron and ion modes are expected to control turbulent transport in the core of both L- and H-mode plasmas. However the change in boundary conditions affects the domain that is explored in the stability diagram (figure 1). Since the edge temperature and density become higher at the transition, the logarithmic gradients are lower in the core of H-mode plasmas.

3. Particle transport

3.1. Theoretical understanding of particle transport

The particle flux of the species 's' in a tokamak is traditionally written in the form $\Gamma_s = -D_s \nabla n_s + V_s n_s$, where V_s is the pinch velocity, D_s the diffusion coefficient, and n_s the density.

In plasmas without neutral beam injection (NBI), the ionization source is mainly peripheral, so that the particle flux in the core vanishes. As a result, the ratio V_s/D_s is a measure of density peaking $\nabla n_s/n_s$. The diffusion coefficient D_s is found to be larger than the neoclassical (collisional) value in most cases. The situation is less clear for the pinch velocity, since the neoclassical contribution driven by the inductive field, the Ware pinch [12], is rarely negligible in most experiments.

From the theoretical standpoint, two additive terms contribute to the turbulent pinch. One is associated with thermo-diffusion [13, 14], and predicts a pinch velocity proportional to the temperature logarithmic gradient $\nabla T_s/T_s$. The second contribution is proportional to the gradient of the magnetic field (or equivalently the curvature) and is sometimes called the 'turbulence equi-partition' (TEP) term [15–17]. This picture is somewhat misleading since the curvature is not a thermodynamical force, but rather a geometric effect. In other words the actual thermodynamical forces are the gradients of density and temperature multiplied by a geometric factor. This mechanism received some support from two-dimensional simulations of interchange turbulence [18] and ITG/TEM micro-turbulence [19]. The question of particle anomalous pinch has been investigated in two recent papers. One exploits first principles transport models (Weiland and GLF23) [20]. The second approach relies on three-dimensional fluid simulations of micro-turbulence [21]. The link between electron (TEM) modes and particle transport was also investigated in connection with particle density transport barriers in Alcator C-Mod [22]. The physical origin of anomalous pinch comes from compressibility. In the collisionless limit, the actual evolution equation of the density is

$$(\partial_t + \boldsymbol{v}_E \cdot \nabla) n_e = \boldsymbol{V}_{de} \cdot (n_e \nabla \phi - \nabla p_e). \tag{4}$$

The compressibility terms in the rhs of this equation lead to non-diagonal contributions in the quasi-linear flux:

$$\Gamma_e = -f_t D_{ql} \left\{ \frac{\mathrm{d}n_e}{\mathrm{d}r} + C_q \frac{2}{R} n_e - C_T \frac{\mathrm{d}T_e}{T_e\,\mathrm{d}r} n_e \right\}. \tag{5}$$

The first term is a conventional diffusion, where D_{ql} is the quasi-linear expression (3). The second term in expression (5) corresponds to the curvature pinch. In the case of cold electrons (vanishing pressure), equation (4) indicates that the density is fully determined by the fluctuations of the electric potential and curvature drift. For trapped electrons, the advection term on the rhs of equation (4) must be replaced by the precession frequency, with the important result $C_q = \lambda_e = 1/4{+}2s/3$. Hence the curvature pinch velocity is proportional to the magnetic shear. This is consistent with the TEP theory [15–17]. When electron modes are dominant, $C_q = \lambda_i = \langle \cos(\theta) + s\theta \sin(\theta) \rangle$, i.e. is linked to the ion vertical drift velocity. The dependence on magnetic shear depends on the degree of localization of modes on the low field side. For ballooning modes, i.e. a turbulence localized close to $\theta = 0$, a dependence on magnetic shear persists since $\lambda_i \approx 1 + (s - 1/2)\langle \theta^2 \rangle$.

The third term of equation (5) is the contribution of thermo-diffusion. The expression of C_T is quite intricate. It is positive in a regime dominated by ion modes and decreases when moving to a regime dominated by electron modes. This transition occurs with increasing ratio of electron to ion heating power. Turbulence simulations indicate that C_T changes sign when this ratio is high enough as shown in figure 2.

Collisional detrapping plays an important role in this problem. It was shown in [20] that the ratio V/D decreases with collisionality. This process is effective when the detrapping collision frequency, ν_{ei}/ε, becomes larger than $(k_\perp \rho_i) v_{Ti}/R$, which measures the electron precession frequency times a typical toroidal wave number. An effective collision frequency was defined in [20] as $\nu_{eff} = (5/2)^{1/2} \nu_{ei} R/(T_e/m_i)^{1/2}$. It is stressed here that the parameter ν_{eff} differs significantly from the conventional parameter $\nu^* = \nu_{ei} q R/\varepsilon_a^{3/2} v_{Te}$ for neoclassical transport.

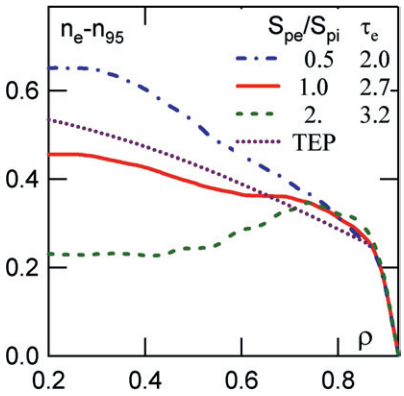

Figure 2. Density profiles calculated with TRB turbulence simulations when varying the ratio of electron to ion heating $S_{pe}/S_{pi} = 0.5$, 1 and 2. The corresponding values of $\tau_e = \nabla T_e/\nabla T_i$ at $r/a = 0.5$ are indicated [21].

A deuterium plasma with $q = 1.5$, $\varepsilon_a = 0.3$ and $\nu_{eff} = 1$ is characterized by a parameter ν^* of the order of 0.1, i.e. is in the weakly collisional regime for neoclassical transport. Also, the density normalized to the Greenwald density (density limit) [23] is used sometimes to characterize the collisionality. However it is not a dimensionless quantity. Therefore it does not behave in the same way as ν_{eff} when using a similarity principle to extrapolate results to a next step device: plasmas close to the density limit are collisonal ($\nu_{eff} > 1$) in present devices, whereas they will be collisionless ($\nu_{eff} < 1$) in ITER.

3.2. Experimental results

Previous experimental results were quite contradictory regarding the particle pinch effect. Density profiles were found to be consistent with the Ware pinch only in ASDEX-Upgrade [24] and JET [25] for plasmas at high density in the H-mode. On the other hand, a turbulent pinch was invoked to explain L-mode density profiles in TCV and TEXTOR [26, 27]. Recent experiments have clarified this question in many aspects.

A first class of results deals with plasmas in the absence of a Ware pinch. The density profiles are peaked in L-mode with zero loop voltage in TORE SUPRA [28], TCV [29] and JET [35]. In TORE SUPRA, the database includes plasmas with a duration of up to 390 s, i.e. much larger than a current diffusion time. Thus both the inductive field and the Ware pinch velocity vanish everywhere. The ionization source was peripheral in these plasmas (no core fuelling), so that a turbulent pinch seems to be the most likely explanation for this behaviour (figure 3). A turbulent pinch was also invoked to explain density profiles in JET [30] and DIII-D [17] L-mode plasmas. At JET, both steady-state regimes and transients (pellet injection) were analysed [30].

Collisionality was found to play a key role in H-mode plasmas. Many plasmas are close to the density limit, in a regime of collisionality where theory predicts small values of V/D [20]. On the other hand, theory predicts finite density peaking at low collisionality. This appears to be the case in ASDEX-Upgrade [20] and JET [31, 32] (figure 4). However two difficulties must be mentioned. First, the ionization source is not always negligible in the plasma core (especially at a low density). Second, any steady-state density profile can be reproduced with a Ware pinch only if the diffusion coefficient is low enough. This lower bound is usually translated into a ratio of diffusion coefficient to electron heat diffusivity D/χ_e, χ_e being easier

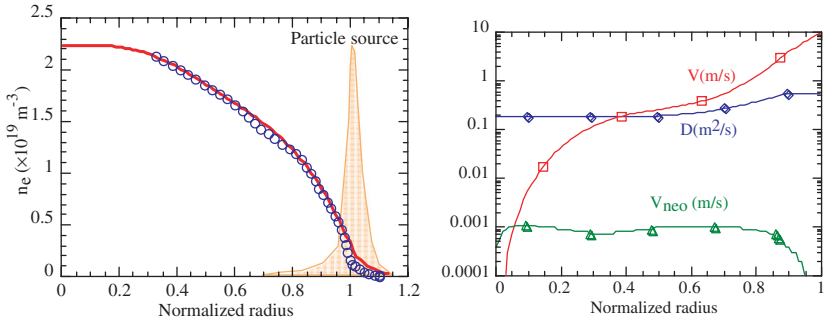

Figure 3. One-dimensional simulation of discharge #30428 in TORE SUPRA, at $t = 30$ s. Left panel: density profile (——, simulation; ○, reflectometry measurements). Right panel: particle pinch velocity (–□–, m s^{-1}) and diffusion coefficient (–◇–, m^2 s^{-1}) used to reproduce the measured density profile. Triangles show the profile of the neoclassical pinch velocity [28].

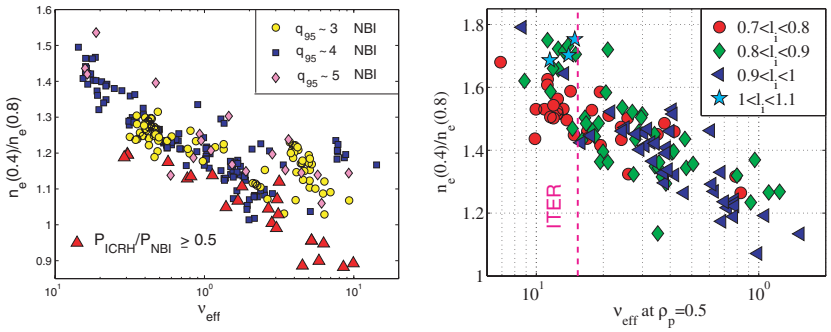

Figure 4. Density peaking versus $\nu_{\rm eff} = (5/2)^{1/2}\nu_{\rm ei}R/(T_{\rm e}/m_{\rm i})^{1/2}$ in ASDEX-Upgrade [20] and JET [31]. Plasmas are in H-mode.

to determine from experiment than D. At JET, the ionization source alone is not large enough in collisionless plasmas ($\nu_{\rm eff} < 1$) to reproduce the density profile unless $D/\chi_{\rm e}$ is smaller than 0.2. This value is lower than predicted by theory [32]. Also, analysis of trace tritium leads to a pinch velocity of tritium that is close to the neoclassical value at high density and much larger at low density [33,34]. Given the uncertainties, these results suggest that density profiles in ITER may be more peaked than assumed. Theory predicts a density gradient length that should be of the order of $-R\nabla n_{\rm e}/n_{\rm e} = 3$ in the confinement zone [38].

A second class of experiments aims at testing the expression (equation (5)) of particle flux. A series of experiments combining current drive and heating has been undertaken at JET in the L-mode to decouple the effects of curvature and thermo-diffusion [31, 35]. The result is shown in figure 5. The density peaking increases with internal inductance, i.e. with the peakedness of the current profile. This is consistent with a curvature pinch term that depends on the magnetic shear. On the other hand there is no indication of thermo-diffusion. The present interpretation is that the gradients lie in a region where ion (ITG) and electron (TEM) modes coexist, hence in a region where $C_{\rm T}$ is close to zero. This is indeed corroborated by stability analysis. A similar result has been found in TORE SUPRA [36].

A related question is the common observation in tokamaks of density profile flattening with radio-frequency (RF) heating. Besides MHD effects, which do not seem to play a dominant

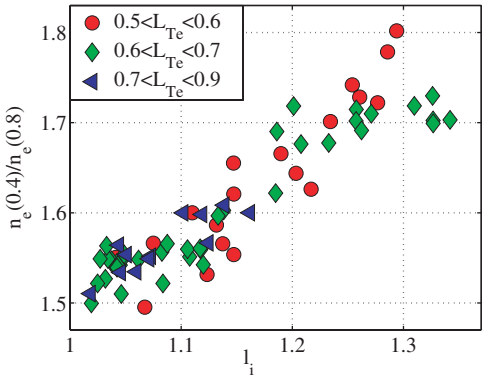

Figure 5. Peakedness of density profiles in JET versus internal inductance for different electron temperature gradient lengths in L-mode (from [31]).

role, two explanations based on turbulent transport have been proposed up to now:

— an outward pinch due to dominant electron (TEM) turbulence;
— an increase of turbulent diffusion at constant or decreasing pinch velocity [37].

Both explanations are possible, as shown recently in ASDEX-Upgrade [38]. The first one is expected in low-collisionality plasmas, with electron heating. Fluid simulations then predict a reversal of the anomalous pinch velocity. The second explanation applies when the pinch velocity is mainly neoclassical since heating should reduce the inductive field and increase the turbulent diffusion. Such behaviour may occur in plasmas at high collisionality, or in the core region, where the anomalous pinch velocity is small [36]. RF heating also flattens impurity profiles (see for instance [39]).

4. Heat transport

Predicting the temperature of a fusion plasma is obviously crucial for designing a reactor. Two main strategies have been followed up to now. The first line of research relies on the development of scaling laws using a multi-machine database in the frame of the International Tokamak Physics Activity (ITPA). The similarity principle is a powerful tool for reducing the uncertainties of scaling laws [8, 9]. The dependence on plasma β and collisionality has been recently revisited, with important consequences for our theoretical understanding [40, 41]. A more sophisticated approach to describing global confinement consists in separating the edge and core contributions, leading to two-term scaling laws that have recently been proposed by the ITPA-CDBM group [42]. The second line of research makes use of transport models complemented by linear stability analysis and turbulence simulations. Turbulence simulations are time consuming and cannot be run on a routine basis to analyse experiments. However, beyond their usefulness in investigating fundamental questions such as intermittency, turbulence simulations can be used to constrain transport models based on quasi-linear and mixing length assumptions (see section 2). Examples of transport models are RLW [43], Weiland [2, 5], IFS-PPPL [44], GLF23 [6], mixed Bohm–gyroBohm [45], Multi-Mode (MMM) [46] and OHE [47] models. In practice, the mixed Bohm–gyroBohm, Weiland and GLF23 models are the most widely used (MMM is a variant of the Weiland model) [48–50]. A simpler picture emerges if turbulent transport becomes very large when gradients cross the stability threshold. The profiles then stay marginally stable, i.e. the gradients are stuck to their

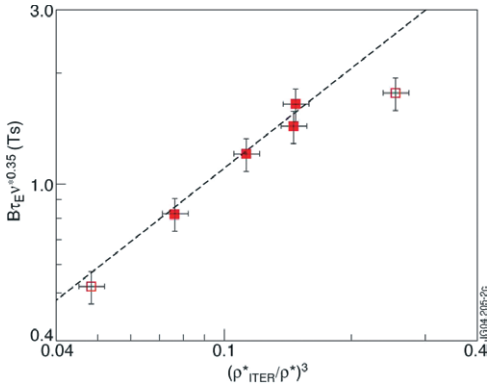

Figure 6. Normalized confinement time, $\nu_*^{0.35} B\tau_E$, versus $[\rho_*/\rho_{*ITER}]^{-3}$ in JET plasmas [67].

critical value. This is called 'profile stiffness' [51]. In practice, only part of the profile is close to marginal stability. This concept is helpful in interpreting experiments [52–57], when combined with linear stability analysis. The Weiland and GLF23 models provide values of linear growth rates. However, they are based on fluid equations, which often predict values for the threshold that are too low. In fact the GLF23 model uses modified fluid equations to correct this drawback. Still, the most accurate procedure for calculating growth rates is to solve a kinetic equation to determine the plasma response. The most widely used tools in Europe are the GS2 [58] and KINEZERO [59] codes. An intermediate approach between predictive transport modelling and strong profile stiffness consists in using a semi-empirical critical gradient model [60–64]. Such a model is characterized by three parameters only and will be used here to illustrate various concepts. The identification of these parameters is made possible by analysing experiments where the heating source is modulated. Profile modulations give access to the heat pulse diffusivity $\chi_{hp} = \chi + \nabla T \partial\chi/\partial\nabla T$ and thereby provide a stringent test of transport models [65]. This section presents recent results related to dimensionless scaling laws and analysis of modulation experiments in several devices.

4.1. Global confinement—dimensionless scaling laws

The IPB(y, 2) scaling law for global confinement time in the H-mode can be written in the dimensionless form [66] $B\tau_E \propto \rho_*^{-2.7}\beta^{-0.9}\nu_*^{-0.01}$ (the magnetic field, B, comes from a normalization of time to the cyclotron frequency). A gyroBohm scaling law based on collisionless electrostatic turbulence predicts $B\tau_E \propto \rho_*^{-3}$: hence the long established conclusion that the scaling law in the H-mode is close to the gyroBohm expectation. On the other hand, the strong dependence on β suggests that electromagnetic effects are important, either in turbulence itself or via MHD effects. This picture has radically changed recently following dedicated experiments in DIII-D and JET [40, 41], which lead to the expression $B\tau_E \propto \rho_*^{-3}\beta^{-0.0}\nu_*^{-0.35}$, as illustrated in figure 6. This new scaling is even closer to the gyroBohm prediction and is consistent with electrostatic turbulent transport. Increasing the collisionality is found to be detrimental. This behaviour is somewhat surprising in view of the expected stabilizing effect of electron collisional detrapping. Damping of zonal flows is a possible explanation. It may also reflect neoclassical effects in the edge pedestal [67].

An alternative approach for H-mode plasmas is a two-term scaling law proposed by the ITPA-CDBM group, which separates contributions from the pedestal and core plasma [42]. Two versions exist that correspond to different hypotheses on the physics underlying the

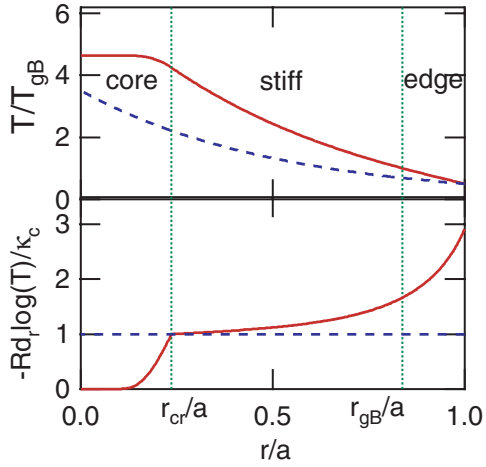

Figure 7. Calculated normalized temperature and its logarithmic derivative. The dashed line corresponds to a profile that is marginally stable everywhere.

confinement in the pedestal region. The first one assumes that the edge confinement is controlled by thermal conduction, while the second relies on an MHD β limit within the pedestal region. In terms of accuracy, these two models are equivalent. Considering the model with MHD limited edge, it is found that the scaling law of the energy content in the bulk region is

$$W_{\mathrm{ITPA,bulk,MJ}} = 0.45 M^{0.34} \kappa^{-0.34} \left(\frac{1+\kappa^2}{2}\right)^{0.68} \varepsilon_{\mathrm{a}}^{3.32} R^3 q_{\mathrm{a}}^{-0.68} B_{\mathrm{T}}^{0.81} n_{\mathrm{a},19}^{0.59} P_{\mathrm{MW}}^{0.42}, \tag{6}$$

where κ is the elongation, M the mass number, $n_{\mathrm{a},19}$ the density (in units of 10^{19} m^{-3}) and P_{MW} the additional power (in MW). The corresponding normalized confinement time $\mathrm{B}\tau_{\mathrm{E}}$ scales as $\rho_*^{-3}\beta^{0.05}$. Again it is close to a collisionless electrostatic gyroBohm scaling law.

4.2. Profile stiffness and critical gradient model

The notion of marginal stability can be illustrated with a simplified transport model. Assuming gyroBohm scaling and electrostatic turbulence (see section 2), a critical gradient model is of the form (for each species)

$$\chi_{\mathrm{T}} = \chi_{\mathrm{gB}} \left[\chi_{\mathrm{s}} \left(\frac{-R\partial_r T}{T} - \kappa_{\mathrm{c}} \right) H \left(\frac{-R\partial_r T}{T} - \kappa_{\mathrm{c}} \right) + \chi_0 \right], \tag{7}$$

where $\chi_{\mathrm{gB}} = q^{\nu}(T/eB)\rho_{\mathrm{s}}/R$. Here, χ_{s} is a number that characterizes the stiffness, κ_{c} is the instability threshold and $H(x)$ is a Heaviside function. A strong stiffness corresponds to a large value of χ_{s}. It is also assumed that a finite diffusivity persists when the gradient is below the threshold, with an amplitude χ_0. The safety factor q accounts for the improvement in confinement with plasma current. Simulations of ion turbulence [6] and recent dedicated experiments [68] justify this choice. The value $\nu = \frac{3}{2}$ is presently the best compromise between various experiments. A detailed analysis of this model shows that the plasma is divided into three regions (see figure 7): the edge, stiff and core regions [44, 64]. The temperature is low at the edge and its logarithmic gradient is well above the threshold. In the stiff region, the temperature increases and its logarithmic gradient is close to the threshold value. An

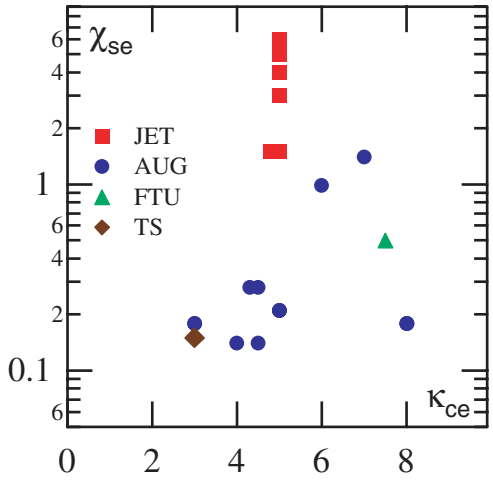

Figure 8. Electron stiffness $\chi_{s,e}$ versus threshold $\kappa_{c,e}$ deduced from modulation experiments in ASDEX-Upgrade, JET and TORE SUPRA, and from a scan of the position of ECRH heating in FTU.

approximate solution is the well-known exponential shape $T(r) \approx T(r_{gB})\, e^{\kappa_c (r_{gB}-r)/R}$, where r_{gB} is the radius of transition between the edge and stiff regions. In this region, the temperature increases faster than its gradient (see figure 8). In the core region the logarithmic derivative of the temperature is below the threshold. The transition between the stiff and core regions is sharp and is associated with a discontinuity in the heat pulse diffusivity.

Once integrated over the plasma volume, a critical gradient model leads to the following expression of core energy content,

$$W_{\mathrm{bulk,MJ}} = 0.179 C_{\mathrm{ITPA}} \chi_{\mathrm{s,eff}}^{-2/5} \kappa_c^{-4/5} M^{-1/5} \kappa^{7/5} \left(\frac{1+\kappa^2}{2}\right)^{-2/5} \varepsilon_a^{8/5} R^3 q_a^{-2\nu/5} B_T^{4/5} n_{a,19}^{3/5} P_{\mathrm{MW}}^{2/5}, \tag{8}$$

where C_{ITPA} depends on the edge temperature and the ratio $\kappa_c \chi_s / \chi_0$, and the effective stiffness parameter is $\chi_{s,\mathrm{eff}} = \chi_{s,e} + \chi_{s,i}$. The factor C_{ITPA} is not a constant because a two-term scaling law is not consistent with a critical gradient model. In fact the separation between the edge and core is rigorous if the diffusivity depends on the temperature gradient only. However, variations in C_{ITPA} are moderate [64]. Assuming a threshold $\kappa_c \approx 5$, and a reasonable choice of the geometric parameters, a comparison of equations (6) and (8) leads to $\chi_{s,\mathrm{eff}}$ in the range 0.3–4.5.

4.3. Analysis of modulation experiments

Electron transport has been analysed in detail in ASDEX-Upgrade, JET, FTU, TORE SUPRA and TCV using heat modulation experiments. The analysis has been done using a critical gradient transport model, predictive modelling and stability analysis.

The results obtained with a critical gradient transport model are shown in figure 8. The thresholds range between 3 and 8, which are typical values expected for micro-modes (see for instance figure 1).

The range of variation of the electron stiffness parameter, $\chi_{s,e}$, is wide ($\chi_{s,e} \sim 0.15$–6). In TCV, $\chi_{s,e}$ is also in this range (on the lower side). It was noticed in TCV that the critical

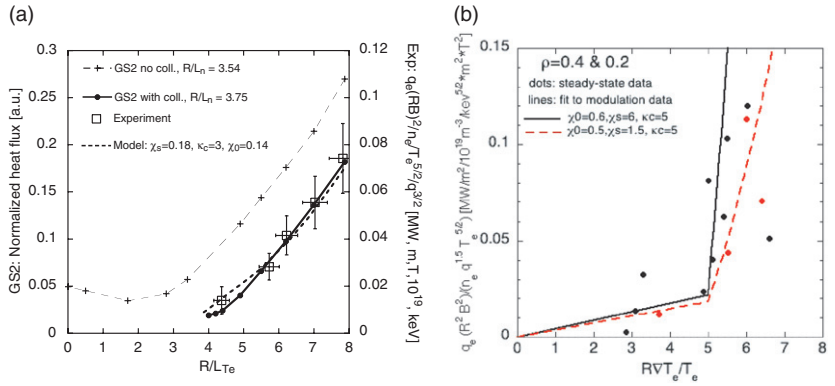

Figure 9. (*a*) Electron heat flux versus logarithmic gradient of electron temperature. Comparison between a quasi-linear estimate calculated with the GS2 stability code and experimental value in ASDEX-Upgrade (from [69]). (*b*) Electron heat flux versus logarithmic gradient of electron temperature in heat modulation experiments at JET with dominant electron heating (- - - -) and significant ion heating (——) (from [50]). Curves for the transport model equation (7) are overlaid.

gradient model does not provide a good fit when the gradient is well above the threshold [63]. Figure 8 indicates that the stiffness is sensitive to the plasma parameters. At JET, the variation in $\chi_{s,e}$ appears to be correlated with the logarithmic gradient of the ion temperature, $-R\nabla T_i/T_i$ [50] (figure 9(*b*)). This points towards a coupling between electron and ion turbulent transport. An interplay between the electron and ion channels can be understood from the stability properties of micro-modes. In the hot electron mode, the main instability is an electron mode (TEM), and a critical gradient model of the form equation (7) seems appropriate. When ion heating increases, ion (ITG) modes become unstable and are ultimately the dominant instability. This means that the background diffusivity quantified by χ_0 in equation (7) for electrons represents the contribution of ion modes when they are unstable. However, the parametric form that has been chosen for the background diffusivity may not be the right one. Also, it is not clear whether contributions of electron and ion modes are additive when both are linearly unstable. Hence equation (7) in its present form may not be appropriate in this regime.

The results obtained with predictive modelling and stability analysis can be summarized as follows. The analysis of modulation experiments in ASDEX-Upgrade using the Weiland model (without off-diagonal terms) shows a good agreement between modelling and data [49]. A more recent study using the GS2 code confirms that TEM is the dominant instability in hot electron plasmas [69]. The quasi-linear electron heat flux is then close to a critical gradient model formulation, provided collisions and density gradient effects are accounted for (figure 9(*a*)). Modelling of heat modulation experiments has been undertaken at JET using Weiland and GLF23 transport models [50]. The collisional Weiland model is able to reproduce experimental data. In particular the electron stiffness is found to increase with the ratio of ion to electron power [50] (figure 9(*b*)). On the other hand, the GLF23 model is generally found to reproduce the electron modulated temperature less well [50, 54].

In summary, although figure 8 exhibits a strong variability in the stiffness factor, it appears that theory can be reconciled with experiments when using first principles modelling. Still, several pending issues remain to be solved. In particular, the question of turbulent transport when several branches coexist remains unclear. This issue will be addressed using turbulence simulations in the future.

5. Formation of ITBs

The physics of ITBs is a broad subject that is already covered by several overview papers [70–72]. The present section is dedicated to the very specific question of ITB formation. This is a crucial question in terms of power threshold, which is the amount of power that is necessary to produce a barrier. Two key ingredients are known to play a central role in the physics of ITBs: shear flow and magnetic topology. The velocity shear rate will be small in a reactor at the onset of an ITB, so that the magnetic shear and Shafranov shift will have to be optimized to trigger the ITB. Attention is focused here on electron transport barriers, which are well suited to studying this physics since the velocity shear rate is naturally small in these plasmas. On the other hand, the physics of barriers in reactor plasmas may be different because the ratio of electron to ion temperature is closer to 1.

5.1. Shear flow stabilization

The physics of turbulent transport reduction due to $E \times B$ shear flow is well documented [73–80]. The interested reader may consult overviews on theory [81] and experiments related to shear flow stabilization [82]. Stabilization results essentially from the shearing of turbulent convective cells. An approximate criterion for stabilization is $\gamma_{\mathrm{E}} > \gamma_{\mathrm{lin}}$ [78], where γ_{E} is the shear flow rate defined as [79]

$$\gamma_{\mathrm{E}} = \frac{RB_\theta}{B}\frac{\mathrm{d}}{\mathrm{d}r}\left(\frac{E_r}{RB_\theta}\right) \tag{9}$$

and γ_{lin} is the maximum linear growth rate. Here B_θ is the poloidal magnetic field and E_r is the radial electric field. The radial electric field is constrained by the ion force balance equation,

$$\frac{e_{\mathrm{i}}E_r}{T_{\mathrm{i}}} = \frac{\mathrm{d}n_{\mathrm{i}}}{n_{\mathrm{i}}\mathrm{d}r} + (1-k_{\mathrm{neo}})\frac{\mathrm{d}T_{\mathrm{i}}}{T_{\mathrm{i}}\,\mathrm{d}r} + \frac{V_\varphi}{B_\theta}, \tag{10}$$

where the number k_{neo} depends on the collisionality regime and V_φ is the ion toroidal velocity. Once a barrier is formed, a positive loop takes place where density and ITGs increase, thus boosting the velocity shear rate. The situation is different at the onset of the barrier. The torque will be small in a reactor, so that $V_\varphi \approx 0$. Since typical growth rates are of the order of c_{s}/a, it is found that the ratio $\gamma_{\mathrm{E}}/\gamma_{\mathrm{lin}}$ scales as the normalized gyroradius, ρ_*. This ratio is small in present tokamaks and will be even smaller in next step devices. Hence shear flow alone cannot usually trigger an ITB in the absence of a torque. A reduction in the linear growth rate is necessary. In that respect, electron transport barriers are interesting since the shear flow rate is small in these plasmas (cold ions, no fuelling and no torque). This property has been verified at JET, where a blip of NBI was used in the preheat phase (dominant electron heating) to measure the velocity profile [83, 84].

5.2. A robust mechanism: negative magnetic shear and α stabilization

Negative magnetic shear is known to decrease the interchange drive [85]. This effect is enhanced by the Shafranov shift of magnetic surfaces (also called α effect, $\alpha = -q^2R\,\mathrm{d}\beta/\mathrm{d}r$ is a measure of the Shafranov shift) [86, 87]. In fact this physics is related to the stability of MHD ballooning modes [88] and the 'access to second stability' (see for instance [89]). For electron modes (TEM), it takes a subtle form as it corresponds to a reversal of curvature drift when $s < -3/8$. This leads to a fully stable situation in terms of interchange stability [7]. This value also corresponds to a reversal of the curvature pinch velocity (see section 3). Since stabilization and pinch reversal occur for the same value of the magnetic shear, a reversal of

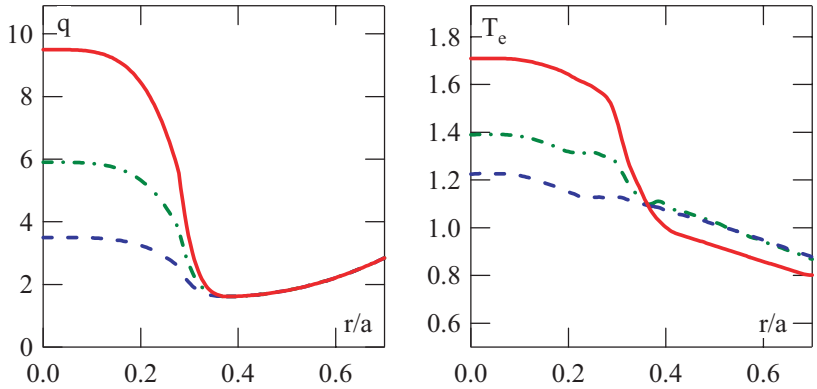

Figure 10. Profiles of safety factor and electron temperature calculated with the TRB turbulence code [91].

curvature pinch is not observable (in other words, the particle pinch should be neoclassical for $s < -3/8$). This stabilization scheme has been tested with the help of kinetic [90] and fluid simulations. An electron transport barrier appears when the magnetic shear is negative, as shown in figure 10 [91]. This effect is amplified for values of α of the order of unity. For electron modes, theory predicts stability when $s < 3\alpha/5–3/8$ [92]. The α effect was found to be important for barrier triggering in DIII-D, but not in JT-60U or JET [93]. It was shown in the same work that the Weiland model does not always predict ITB formation because the effect of magnetic shear is not strong enough. The GLF23 model does predict ITB formation [94], although differences between measured and modelled profiles appear in the radial location and/or the height of the barrier [93].

Stabilization with negative magnetic shear is consistent with the onset of an electron barrier in JET during the preheat phase with LHCD [83]. The mechanism is found to work provided the heating power is localized in the core [95]. It is also consistent with the early observation of electron barriers (LHEP mode) on TORE SUPRA [96], FTU [97], TCV [98] and more recently on ASDEX-Upgrade [99]. Although not the focus of this section, it is worth noting that a similar effect exists for ions, which comes from the shear dependence of the ion curvature averaged over the mode structure $\lambda_i = \langle \cos(\theta) + (s\theta - \alpha \sin(\theta)) \sin(\theta) \rangle$. This physics has been studied in detail and will not be addressed further here (see for instance [100]).

5.3. Why negative magnetic shear cannot be the only mechanism

An explanation based on negative magnetic shear is unable to explain the full range of barriers observed in JET. There are two reasons at least for this: the role of rational $q_{\min}$ and the coexistence of several barriers. The favourable role of a low order rational value of the minimum safety factor in reversed shear plasmas due to the observation of Alfvèn wave cascades has recently been confirmed [101, 102]. Coexistence of barriers has been observed in both electron and ion channels at JET. A transition is often observed between a single barrier localized at negative shear and a double barrier, when $q_{\min}$ crosses a low order rational number (see figure 11). Also, the radial location of ITBs in JET is correlated with the $s = 0$ magnetic surface [103]. Three explanations have been proposed to explain this behaviour:

(i) The onset of MHD modes located at rational values of q that generate a localized velocity shear [104]. An alternative is based on a loss of fast ions due to MHD that leads to a shear flow [105].

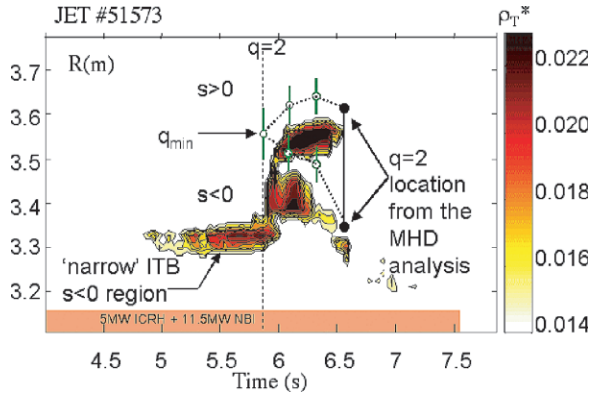

Figure 11. Contours of $\rho_T^* = (m_i T_e)^{1/2}/(eBL_{Te})$ of JET pulse #51573 (from [104]).

(ii) Turbulent flow generation enhanced close to rational q values. This explanation does receive some support from electromagnetic turbulence simulations with the CUTIE code [106]. These simulations also show that low wave number modes modify the q profile near rational values, thus further lowering the magnetic shear locally.

(iii) The existence of gaps in the density of magnetic surfaces where the safety factor is rational (these are regions where modes tend to be localized because of resonances). This gap is wider when q_{min} is close to a low order rational number. Also, several gaps may appear simultaneously [107].

The third explanation has been questioned by recent turbulence simulations with the gyrokinetic code GYRO, which do not find any sign of gaps, nor a special role of zero magnetic shear $s = 0$ [108]. The explanation based on MHD does find some support from the correlation observed in JET between ITB formation and MHD activity in positive (optimized) shear plasmas [104]. MHD activity is not always observed in reversed shear plasmas, apart from the Alfvèn cascade itself. However, tearing modes located at $q = 2$ surfaces may be difficult to detect. An explanation based on a turbulent dynamo and localized velocity shear is still being discussed and is difficult to verify experimentally, although large transients in the $E \times B$ flow were observed in TFTR [109].

6. Conclusion

Progress has been made in understanding particle transport in tokamaks. Theory predicts that both thermo-diffusion and magnetic field curvature contribute to the turbulent pinch. Also, the curvature pinch depends on the magnetic shear and the peaking factor decreases with collisionality. These predictions have been tested against experimental results in several devices. Plasmas with peaked density profiles and no Ware pinch were produced in TORE SUPRA and TCV, thus pointing towards the existence of a turbulent pinch in the L-mode. It has been verified also that the pinch velocity increases with magnetic shear in JET, TORE SUPRA and TCV L-mode plasmas. In the H-mode, the density peaking is sensitive to the collisionality as found in ASDEX-Upgrade and JET. At high collisionality, the pinch velocity is close to the Ware value, whereas it is larger at low collisionality. This suggests that density profiles in ITER may be more peaked than planned. RF heating is found to flatten density profiles. When the collisionality is large, this is interpreted as an increase in the turbulent

diffusion coefficient, while the pinch velocity stays close to the neoclassical value. For low density plasmas, the interpretation rather relies on the weakening (and maybe reversal) of pinch velocity predicted by theory when the turbulence moves from ion to electron dominant heating.

Progress has been made in the development of dimensionless scaling laws and assessment of transport models using heat modulation experiments. Recent experiments on DIII-D and JET show that the dimensionless scaling law of energy confinement is consistent with electrostatic turbulent transport. A low collisionality is found to improve the confinement. This behaviour remains unexplained. These results lead to a prediction of confinement that will be better than expected in ITER in the domain of high beta plasmas. Heat modulation experiments have been performed at JET, ASDEX-Upgrade, TORE SUPRA, FTU and TCV. These experiments have been analysed using a critical gradient transport model, stability, analysis and predictive modelling. The instability thresholds are found to be in the expected range for micro-instabilities in tokamaks. The electron stiffness is found to cover a wide range of variation. However the Weiland transport model is able to reproduce experimental data both in ASDEX-Upgrade and in JET. Also, kinetic stability analysis is consistent with transport modelling and a critical gradient model for hot electron plasmas in ASDEX-Upgrade. At JET a correlation was found between the electron stiffness and the ITG length. This observation suggests that some interplay exists between electron and ion heat channels. The applicability of a critical gradient model in the case where ion and electron modes are linearly unstable will thus have to be further investigated. No firm conclusion can yet be drawn regarding the profile stiffness in ITER.

Finally the question of triggering ITBs has been addressed by analysing electron transport barriers, which are characterized by a low mean shear flow. It is confirmed that negative magnetic shear, combined with the Shafranov shift, is a robust stabilizing mechanism. However, some well established features of internal barriers are not explained by theory, in particular the role of rational values of the minimum safety factor and the existence of multiple barriers. Tailoring the current profile may well provide the most efficient way of producing ITBs in ITER, since the mean velocity shear rate will be moderate in these plasmas. This will require efficient tools for modifying the shape of the plasma current density.

References

[1] Horton W 1999 *Rev. Mod. Phys.* **71** 735
[2] Weiland J 2000 *Collective Modes in Inhomogeneous Plasmas* (Bristol: Institute of Physics Publishing)
[3] Rewoldt G, Tang W M and Hastie R J 1987 *Phys. Fluids* **30** 807
[4] Jenko F, Dorland W, Kotschenreuther M and Rogers B N 2000 *Phys. Plasmas* **7** 1904
[5] Nordman H, Weiland J and Jarmen A 1990 *Nucl. Fusion* **30** 983
[6] Waltz R E *et al* 1997 *Phys. Plasmas* **4** 2482
[7] Kadomtsev B B 1975 *Sov. J. Plasma Phys.* **1** 295
[8] Connor J W and Taylor J B 1977 *Nucl. Fusion* **17** 1047
[9] Kadomtsev B B and Pogutse O P 1970 *Reviews of Plasma Physics* vol 5, ed M A Leontovitch (New York: Consultant Bureau) p 249
[10] Diamond P H *et al* 1998 *Proc. 17th IAEA Fusion Energy Conf.* IAEA-CN-69/TH3/1
[11] Falchetto G and Ottaviani M 2004 *Phys. Rev. Lett.* **92** 25002
[12] Ware A A 1970 *Phys. Rev. Lett.* **25** 916
[13] Coppi B and Spight C 1978 *Phys. Rev. Lett.* **41** 551
[14] Tang W *et al* 1986 *Phys. Fluids* **29** 3715
[15] Yankov V V 1994 *JETP Lett.* **60** 171
[16] Isichenko M B, Gruzinov A V and Diamond P H 1996 *Phys. Rev. Lett.* **74** 4436
[17] Baker D R and Rosenbluth M N 1998 *Phys. Plasmas* **5** 2936
[18] Naulin V, Nycander J and Juul Rasmussen J 1998 *Phys. Rev. Lett.* **81** 4148

[19] Nordman H, Weiland J and Jarmen A 1990 *Nucl. Fusion* **30** 983
[20] Angioni C *et al* 2003 *Phys. Plasmas* **10** 3225
Angioni C *et al* 2003 *Phys. Rev. Lett.* **90** 205003-1
[21] Garbet X *et al* 2003 *Phys. Rev. Lett.* **91** 035001
[22] Ernst D R *et al* 2004 *Phys. Plasmas* **11** 2637
[23] Greenwald M *et al* 1988 *Nucl. Fusion* **28** 2199
[24] Stober J *et al* 2001 *Nucl. Fusion* **41** 1535
[25] Valovic M *et al* 2000 *Plasma Phys. Control. Fusion* **44** 1911
[26] Weisen H *et al* 2002 *Nucl. Fusion* **42** 136
[27] Tokar M Z, Ongena J, Unterberg B and Weynants R R 2000 *Phys. Rev. Lett.* **84** 895
[28] Hoang G T *et al* 2003 *Phys. Rev. Lett.* **90** 155002
[29] Zabolotsky A, Weisen H and TCV Team 2003 *Plasma Phys. Control. Fusion* **45** 735
[30] Garzotti L *et al* 2003 *Nucl. Fusion* **43** 1829
[31] Weisen H *et al* 2004 *Proc. 31st EPS Conf. on Plasma Physics (London, 2004)*
[32] Valovic M *et al Plasma Phys. Control. Fusion* **46** B557
[33] Zastrow K-D *et al* 2004 *Proc. 31st EPS Conf. on Plasma Physics (London, 2004) Plasma Phys. Control. Fusion* **46** B255
[34] Voitsekhovitch I *et al* 2004 *Proc. 31st EPS Conf. on Plasma Physics (London, 2004)*
[35] Weisen H *et al* 2004 *Plasma Phys. Control. Fusion* **46** 751
[36] Hoang T *et al* 2004 *Phys. Rev. Lett.* **93** 135003
[37] Stober J *et al* 2003 *Nucl. Fusion* **43** 1265
[38] Angioni C *et al* 2004 *Nucl. Fusion* **44** 827
[39] Puaitti M E *et al* 2002 *Plasma Phys. Control. Fusion* **44** 2135
[40] McDonald D C *et al* 2004 *Plasma Phys. Control. Fusion* **46** A215
[41] Petty C C *et al* 2004 *Phys. Plasmas* **11** 2514
[42] Cordey G *et al* 2003 *Nucl. Fusion* **43** 670
[43] Rebut P H, Lallia P P and Watkins M L 1989 *Plasma Physics Control. Nucl. Fusion Research 1998: Proc. 12th Int. Conf. (Nice, 1988)* vol II (Vienna: IAEA) p 191
[44] Kotschenreuther M, Dorland W, Beer M A and Hammett G W 1995 *Phys. Plasmas* **2** 2381
[45] Erba M *et al* 1997 *Plasma Phys. Control. Fusion* **39** 261
[46] Zhu P, Bateman G, Kritz A H and Horton W 2000 *Phys. Plasmas* **7** 2898
[47] Ottaviani M, Horton W and Erba M 1997 *Plasma Phys. Control. Fusion* **39** 1461
[48] Parail V *et al* 1997 *Nucl. Fusion* **37** 481
[49] Tardini G *et al* 2002 *Nucl. Fusion* **42** L11
[50] Mantica P *et al* 2004 *Proc. 31st EPS Conf. on Plasma Physics (London, 2004)*
Mantica P *et al* 2003 *Proc. 30th EPS Conf. on Plasma Physics (St Petersburg, 2003)*
[51] Coppi B and Sharky N 1981 *Nucl. Fusion* **21** 1363
[52] Ryter F *et al* 2001 *Phys. Rev. Lett.* **86** 2325
[53] Hoang G T *et al* 2001 *Phys. Rev. Lett.* **87** 125001
[54] Mantica P *et al* 2002 *Plasma Phys. Control. Fusion* **44** 2185
[55] Baker D R *et al* 2001 *Phys. Plasmas* **8** 4128
[56] Peeters A G 2002 *Nucl. Fusion* **42** 1376
[57] Mikkelsen D R *et al* 2003 *Nucl. Fusion* **43** 30
[58] Kotschenreuther M *et al* 1995 *Phys. Plasmas* **2** 2381
[59] Bourdelle C *et al* 2002 *Nucl. Fusion* **42** 892
[60] Imbeaux F, Ryter F and Garbet X 2001 *Plasma Phys. Control. Fusion* **43** 1503
[61] Ryter F *et al* 2003 *Nucl. Fusion* **43** 1396
[62] Mantica P 2002 *Proc. 19th IAEA Fusion Energy Conf. (Lyon, 2002)*
[63] Camenen Y, Pochelon A, Ryter F and Coda S 2003 Electron heat transport studies under intense EC heating in TCV *IAEA Technical Meeting on ECRH Physics and Technology for ITER (F1-TM-26015) (Kloster Seeon, Germany, July 2003) CRPP Lausanne Report* LRP 768/03
[64] Garbet X *et al* 2004 *Plasma Phys. Control. Fusion* **46** 1351
[65] DeBoo J *et al* 1999 *Nucl. Fusion* **39** 1935
[66] Kardaun O J W F *et al* 2001 *Fusion Energy 2000: Proc. 18th Int. Conf. (Sorrento, 2002)* (Vienna: IAEA)
[67] Cordey G *et al* 2004 *Proc. 31st EPS Conf. on Plasma Physics (London, 2004)*
[68] Petty C C, Kinsey J E and Luce T C 2004 *Phys. Plasmas* **11** 1011
[69] Peeters A G, Angioni C, Apostoliceanu M, Jenko F, Ryter F and the ASDEX Upgrade Team to be submitted
[70] Wolf R C 2003 *Plasma Phys. Control. Fusion* **45** R1

[71] Connor J W *et al* 2004 *Nucl. Fusion* **44** R1
[72] Challis C *Plasma Phys. Control. Fusion* **46** B23
[73] Itoh S-I and Itoh K 1988 *Phys. Rev. Lett.* **60** 2276
[74] Shaing K C and Crume E C 1989 *Phys. Rev. Lett.* **63** 2369
[75] Biglari H, Diamond P H and Terry P W 1990 *Phys. Fluids* B **2** 1
[76] Hamaguchi S and Horton W 1992 *Phys. Fluids* B **4** 319
[77] Staebler G M, Hinton F L, Wiley J C, Dominguez R R, Greenfield C M, Gohil P, Kurki-Suonio T K and Osborne T H 1994 *Phys. Plasmas* **1** 909
[78] Waltz R E, Kerbel G D and Milovitch J 1994 *Phys. Plasmas* **1** 2229
[79] Hahm T S and Burrell K H 1995 *Phys. Plasmas* **2** 1648
[80] Figarella C *et al* 2003 *Phys. Rev. Lett.* **90** 015002
[81] Terry P W 2000 *Rev. Mod. Phys.* **72** 109
[82] Burrell K H 1999 *Phys. Plasmas* **6** 4418
[83] Hogeweij G M D *et al* 2002 *Plasma Phys. Control. Fusion* **44** 1155
[84] Conway G D *et al* 2002 *Plasma Phys. Control. Fusion* **44** 1167
[85] Drake J F *et al* 1996 *Phys. Rev. Lett.* **77** 494
[86] Beer M *et al* 1997 *Phys. Plasmas* **4** 1792
[87] Bourdelle C *et al* 2003 *Phys. Plasmas* **10** 2881
[88] Connor J W, Hastie R J and Taylor J B 1978 *Phys. Rev. Lett.* **40** 396
[89] Coppi B, Ferreira A, Mark J-W-K and Ramos J J 1979 *Nucl. Fusion* **19** 715
[90] Bottino A 2004 *PhD Thesis* Lausanne
[91] Baranov Y *et al* 2004 *Plasma Phys. Control. Fusion* **46** 1181
[92] Maget P, Garbet X, Géraud A and Joffrin E 1999 *Nucl. Fusion* **39** 949
[93] Tala T *et al Nucl. Fusion* submitted
[94] Kinsey J *et al* 2002 *Phys. Plasmas* **9** 1976
[95] Kirneva N *et al* 2004 *Proc. 31st EPS Conf. on Plasma Physics (London, 2004)*
[96] Moreau D and the TORE SUPRA Team 1994 *Proc. 14th Int. Conf. on Plasma Physics and Controlled Nuclear Fusion Research (Würtzburg, 1992)* vol I (Vienna: IAEA) p 649
Litaudon X *et al* 1996 *Plasma Phys. Control. Fusion* **38** 1603
[97] Buratti P *et al* 1999 *Phys. Rev. Lett.* **82** 560
[98] Goodman T P *et al* 2003 *Nucl. Fusion* **43** 1619
[99] Leuterer F *et al* 2003 *Nucl. Fusion* **43** 1329
[100] Budny R *et al* 2003 *Proc. 30th EPS Conf. on Plasma. Phys. Control. Fusion (St Petersburg, 2003)* vol 27A, O-3.4A
[101] Sharapov S *et al* 2002 *Phys. Plasmas* **9** 2027
[102] Joffrin E *et al* 2003 *Nucl. Fusion* **43** 1167
[103] Esposito B *et al* 2003 *Plasma Phys. Control. Fusion* **45** 933
[104] Joffrin E *et al* 2002 *Plasma Phys. Control. Fusion* **44** 1739
[105] Guenter S *et al* 2000 *Proc. 28th EPS Conf. on Plasma Phys. Control. Fusion* vol 25A, p 1006
[106] Thyagaraja A, Knight P J and Loureiro N 2004 *Eur. J. Mech.* B **23** 475
[107] Garbet X *et al* 2003 *Nucl. Fusion* **43** 975
[108] Candy J, Waltz R and Rosenbluth M N 2004 *Phys. Plasmas* **9** 1938
[109] Bell R E *et al* 1998 *Phys. Rev. Lett.* **81** 1429